Available online at www.sciencedirect.com
SCIENCE DIRECT®
International Journal of Solids and Structures 43 (2006) 2497–2512
INTERNATIONAL JOURNAL OF SOLIDS and STRUCTURES
www.elsevier.com/locate/ijsolstr

Study on energy absorbing composite structure made of concentric NiTi spring and porous NiTi

Ying Zhao [a,1], Minoru Taya [a,*], Hiroshi Izui [b]

[a] Department of Mechanical Engineering, University of Washington, Seattle, WA 98105, USA
[b] Department of Aerospace Engineering College of Science and Technology, Nihon University, Chiba, Japan

Received 11 January 2005; received in revised form 16 June 2005
Available online 10 August 2005

Abstract

An energy absorbing composite structure made of a concentric NiTi spring and a porous NiTi rod is investigated in this paper. Both NiTi spring and porous NiTi rod are of superelastic grade. Ductile porous NiTi cylindrical specimens are fabricated by spark plasma sintering. The composite structure exhibits not only high reversible force–displacement relation for small to intermediate loading but also high energy absorbing property when subjected to large compressive load. A model for the compressive force–displacement curve of the composite structure is presented. The predicted curve is compared to the experimental data, resulting in a reasonably good agreement.

Keywords: Energy absorbing material; Composite structure; NiTi spring; Porous NiTi; Spark plasma sintering

1. Introduction

Recently, the energy absorbing structures and materials attracted strong interests in various fields of applications ranging from vehicles, ballistic armor, helmet, sports equipment to clothing. There are two approaches to design high energy absorbing materials and structures: One is to optimize the structures by using ordinary materials, for example thin composite sandwich panels by Kassapoglou (1996), and sandwich plates with truss cores by Xue and Hutchinson (2004) and Wicks and Hutchinson (2004). The other is to design new energy absorbing materials, such as Miyoshi et al. (1999) produced aluminum foam, porous NiTi shape memory alloys. Since the density of porous NiTi is less than that of the solid NiTi, while the

* Corresponding author. Tel.: +1 206 685 2850; fax: +1 206 685 8047.
E-mail addresses: yzhao@u.washington.edu (Y. Zhao), tayam@u.washington.edu (M. Taya).
[1] Tel.: +1 206 6162163; fax: +1 206 6164088.

0020-7683/$ - see front matter
doi:10.1016/j.ijsolstr.2005.06.043

porous NiTi can absorb almost the same energy as the solid NiTi does when they have the same volume, the porous NiTi can be good candidate for energy absorbing material in various fields of applications ranging from aerospace and naval to surgical instruments and medical implant and fixtures. There have been some attempts to design and process porous NiTi, but the porous NiTi in the earlier works proved to be very brittle. Recently we processed a ductile porous NiTi rod by using spark plasma sintering (SPS) method by Kang et al. (2001) where starting NiTi powder of superelastic (SE) grade were used. Due to short processing time inert environment, as-SPS processed porous NiTi was found to be ductile and exhibited SE behavior.

In this paper, we will incorporate both approaches mentioned above, i.e. to design a high energy absorbing composite structure by not only optimizing the structure design, but also designing of energy absorption porous shape memory alloy. We proposed to design a composite structure made of concentric NiTi spring and porous NiTi cylinder where both NiTi are of SE grade. Let us consider a composite structure made of a concentric spring and porous cylinder, both are of superelastic NiTi, Fig. 1. The composite structure is subjected to compressive loading F along the z-direction. In order to design a high energy absorbing material to cover a wide range of compressive loading, we set our criteria: (i) for low to intermediate compressive loading, the composite structure exhibits superelasticity, i.e. the whole structure recovers to its original shape after unloading. (ii) For high compressive loading, the composite structure can absorb a larger amount of energy. Therefore, the proposed composite structure has dual purposes, (i) usable as an impact every absorber repeatedly for low impact energy, and (ii) extra high energy absorber for much larger impact loading. We design the composite structure such that there exists a horizontal gap between the outer spring and inner cylinder and the initial height of the spring is larger than that of the cylinder, Fig. 2(a). Upon compressive loading to the composite structure, the spring supports the compressive loading initially until both of the spring and cylinder have the same height, Fig. 2(b). Under increasing compressive load, the spring shrinks while the cylinder shrinks vertically but swells transversely, then it touches the spring, Fig. 2(c). For further loading, to cope with larger impact loading, the deformation of the composite structure is strongly influenced by the constraint between the spring and cylinder with constrained inner pressure acting on the interface, thereby absorbing a large impact loading.

So far, a lot of modeling work were proposed to simulate the mechanical behaviors of energy absorbing structures and materials. For example, Bart-Smith et al. (2001) proposed a model to simulate the bending deformation of a cellular metal sandwich construction made of aluminum foam. Wicks and Hutchinson

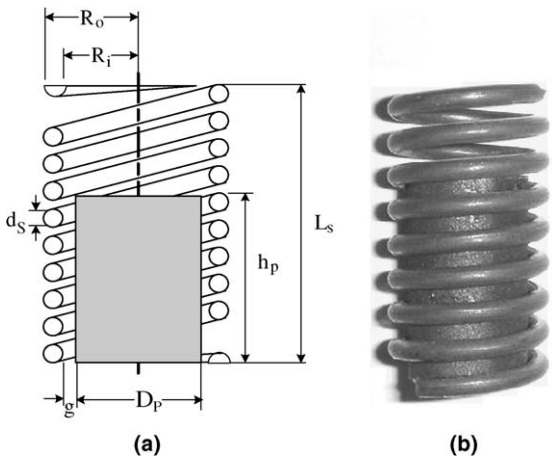

Fig. 1. (a) Sketch and (b) actual picture of the composite structure.

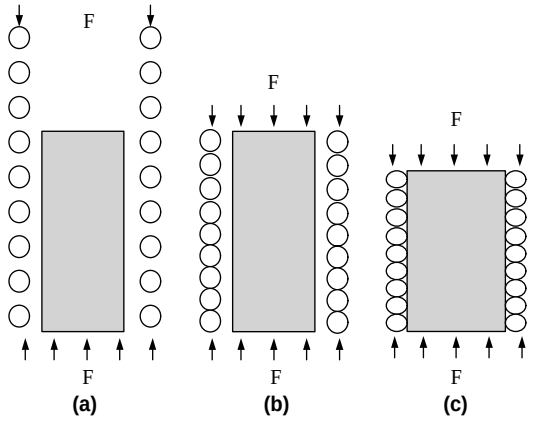

Fig. 2. Three stages of the composite structure under compression, (a) first stage: spring singly takes the load, (b) second stage: the spring shrinks to the same height as that of the rod, (c) the rod expands radially, and touches the inner surface of the spring.

(2001) constructed a model to optimize the truss plates to achieve higher energy absorption. However, there is no model proposed for the energy absorbing structure based on shape memory alloys. Therefore, in this paper, we propose a model aiming at simulation of the sequence of deformation of composite structure made of porous NiTi rod and concentric NiTi spring, Fig. 2 and also the deformation thereafter until the maximum stress and strain reached in the superelastic SME spring cylinder followed by the unloading.

2. Design, processing and characterization of the porous NiTi rod and the composite structure

The composite structure is composed of 13% porosity NiTi rod surrounded by a concentric NiTi spring, Fig. 1. Both of the rod and spring are of superelastic (SE) grade at room temperature. Table 1 shows the dimension of this structure.

Here we shall state briefly the processing and characterization of porous NiTi cylinder and spring both of which are made of NiTi shape memory alloy (SMA) of superelastic grade.

The ingot of NiTi (SE) is provided by Sumitomo metal (Osaka, Japan). After the prealloyed ingot was prepared, the NiTi powders were produced by the Plasma Rotation Electrode Process (P-REP) by Fukuda Metal Co. (Kyoto, Japan), this method is by Kato et al. (1994). Porous NiTi cylinder specimens were made of spark plasma sintering (SPS) system (Sumitomo Coalmine Company, Japan, Model 1040s) where NiTi powder of SE grade (average diameter is 200 μm) were packed in a graphite mold. The NiTi powders in the mold then were sintered by the SPS under pressure of 25 MPa at 800 °C for 5 min in N_2 gas flow. As-SPS processed NiTi specimen has a 13% porosity and it was subjected to the heat treatment at 320 °C for 30 min, followed by water quench to convert it to SE grade, Zhao et al. (2005). Typical cross-section of 13% porosity NiTi is shown in Fig. 3.

Table 1
Dimension of the porous NiTi rod and NiTi spring, see Fig. 1

Porous NiTi rod		NiTi spring							
D_p	h_p	R_o	R_i	L_s	d_s	g	p	α	n
9.0 mm	15.0 mm	6.25 mm	4.6 mm	20.3 mm	1.65 mm	0.1 mm	1.75 mm	5.5°	9

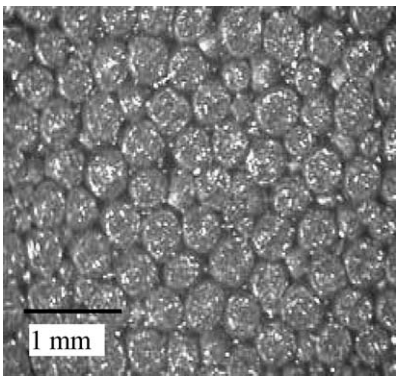

Fig. 3. Uniform cross-section of the 13% porosity NiTi.

The 13% porosity NiTi (hereafter porous NiTi) specimen was subjected to compression test, and its force–displacement curve is given in Fig. 4 where Fig. 4(a) is the force–displacement curve of the single porous NiTi rod under compressive load, Fig. 4(b) shows the force–displacement curve of the composite structure (a porous NiTi rod surrounded by a NiTi helical spring). Both tests are conducted at room temperature. As to the composite structure, before the spring shrinks to the same height of the porous NiTi rod, it is the single rod that supports the compressive load. Therefore, in Fig. 4(b) the forces corresponding to the displacements ranging from 0.0 mm through 5.3 mm remains modest and this range is omitted for the sake of comparison with Fig. 4(a). Fig. 4(b) also shows that after the spring shrinks to the same height as that of the porous NiTi rod, both spring and porous NiTi rod are supporting the load, furthermore, each turn of the spring touches its neighbor turns to make the spring behave like a hollow cylinder. Thereafter, the force increases sharply. Comparing Fig. 4(a) and (b), it is obvious that the composite structure exhibits the capability of supporting large force and displacement. For the porous NiTi rod, the spring plays a roll as a constraint while the porous NiTi rod with a spring surrounded exhibits higher superelastic force, higher fracture point and larger displacement than the single porous NiTi rod without spring surrounded. On the other hand, the porous NiTi rod act as a yoke for the spring, preventing it from asymmetric deformation (i.e. premature buckling) when subjected to large force. Let us example the experimental data of Fig. 4 in terms of energy absorbing (EA) capacity for two different regimes: (i) reversible (superelastic) and (ii)

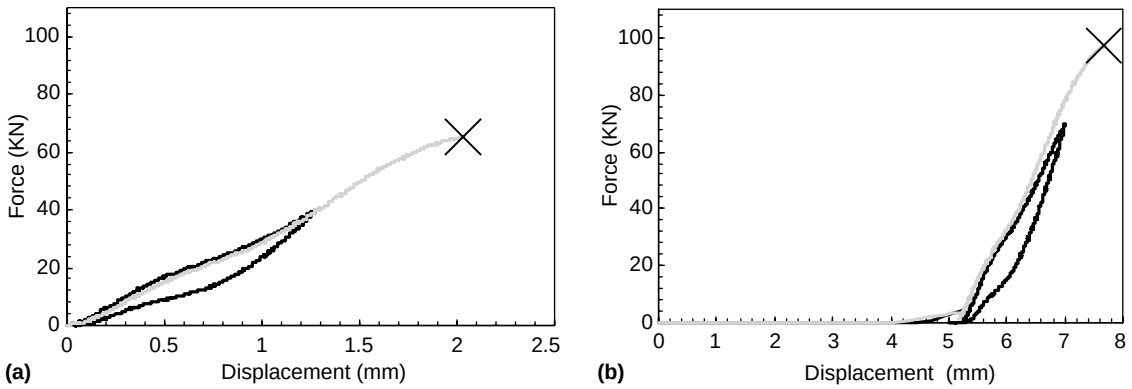

Fig. 4. Force–displacement curve of (a) single porous NiTi rod and (b) composite at room temperature.

Table 2
Comparison of the experimental data of the single porous NiTi rod and composite structure with their dimension shown in Table 1

	Maximum reversible displacement (mm)	Maximum reversible force (kN)	Fracture displacement (mm)	Fracture force (kN)	Specific energy absorption (MJ/Mg)
Single porous NiTi rod	1.29	40.74	2.03	65.15	12.2
Composite	1.71	68.76	2.41	97.21	15.3

irreversible (loading all the way to its fracture point). For the first regime, we define EA as the area surrounded by SE loop while for the second regime, EA is defined by the area underneath the force–displacement curve up to the fracture point marked in the figure by X. The two values of EA are divided by the mass of each specimen to calculate specific EA. The key mechanical data including specific EA are listed in Table 2 of porous NiTi rod and the composite structure. The results of Fig. 4 and Table 2 demonstrate the advantage of using the composite structure as compared with porous NiTi rod above to cope with a wide rage of comprehensive load bearing capacity. In summary, the proposed composite structure has dual use as an efficient energy absorber for both low and high impact loading. It is noted also that the higher strain-rate impact loading, the higher the flow stress of NiTi becomes which maybe considered additional advantage of using NiTi as a key energy absorbing material.

3. Model for predicting the force–displacement curve (FDC) of the composite structure

The force–displacement curve (FDC) of a composite structure has two parts, loading and unloading. The loading curve consists of five kink points and five segments, see Fig. 5. First kink point, A, is the point at which the spring shrinks to the same height as the rod. The second kink point, B, is the point in which the porous NiTi rod exhibits the onset martensite transformation, which is obtained from the experimental FDC of single porous NiTi rod. The third, C, is the point when the rod touches the inner surface of the spring. The fourth, D, is the finish martensite transformation point. The fifth, E, is the onset point of the plastic deformation for the porous NiTi rod. The unloading curve consists of four kink points. The first, F, is the start point of the austenite transformation. The second, G, is the point when the rod detaches the inner surface of the spring. The third, H, is the finish point of austenite transformation. The fourth, I, is the point at which the rod reverses to its original height, which is the same as point A on the loading curve. In this model, the FDC of the porous NiTi rod is set as the reference data and the Young's modulus of the spring is assumed to 70 GPa (it is shear modulus $G_s = 26.3$ GPa).

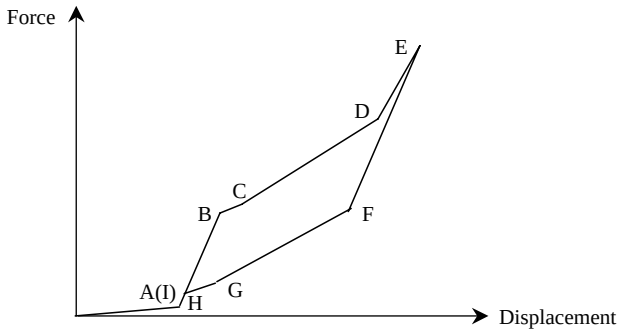

Fig. 5. Idealized force–displacement curve of the composite structure.

3.1. Loading curve

3.1.1. The first stage ($O \rightarrow A$)

The start of this stage is the origin of the FDC. Since the spring is set initially longer than the rod, the spring is the only load bearing member of the composite structure under compressive loading until point A. The force–displacement relation for the NiTi spring is given by Kusaka and Taya (2004).

$$F_s = \frac{G_s d^4}{64 n R_o^3} \delta_s \tag{1}$$

where G_s is the shear modulus of the spring, in this paper it is 26.3 GPa. F_s and δ_s are the force and displacement of the spring, n is number of turns, d and R are defined in Fig. 1. The difference of the length of porous NiTi rod and the spring is the displacement at point A. This displacement is given in Table 4. Therefore, the force at kink point A can be obtained by substituting displacement (i.e. $OA = \delta_A$ in Fig. 5) into Eq. (1) as

$$F_A^s = \frac{G_s d^4}{64 n R_o^3} \delta_A \tag{2}$$

It is noted in Eq. (2) that F_A^s represents the load supported by only the spring of composite structure as in this portion only the spring is taking the applied load.

3.1.2. The second stage ($A \rightarrow B$)

When the spring shrinks to the same height of porous NiTi rod, the second stage starts. As displacement increases, the porous NiTi rod exhibits the onset of stress-induced martensitic transformation point, B. The displacement at B can be found in Table 4. The porous NiTi rod does not touch the inner surface of the spring. Therefore, these two parts (rod and spring) act independently. Because each turn of the spring touches its adjacent turns, it behaves like a hollow cylinder. Hence, from this stage all the way through the stage ($H \rightarrow I$), the spring is assumed to act as a hollow cylinder. Therefore, using the volume of the spring and the hollow cylinder is equal to each other, the equivalent thickness of the hollow cylinder can be obtained. The volume of the spring is

$$V_s = \pi (R_o^2 - R_i^2) d_s n \tag{3a}$$

The volume of the hollow cylinder is given as

$$V_{cyl} = 2\pi R_i h_p t \tag{3b}$$

where t and h_p are the equivalent thickness and height of the hollow cylinder. All of the parameters can be found in Table 1. The equivalent thickness t is calculated by equating Eqs. (3a) and (3b)

$$t = \frac{n(R_o^2 - R_i^2) d_s}{R_i h_p} \tag{3c}$$

The force–displacement relation of the porous NiTi rod can be obtained from the reference FDC of porous NiTi rod, which can be found in Table 4. Since the spring is assumed to be a hollow cylinder, its force at B, F_B, is given as

$$F_B^s = E_s[(R_i + t/2)^2 - R_i^2](\delta_B - \delta_A)/h_p \tag{4}$$

Hence the force applied to the entire composites structure is the summation of the force on the spring and the rod

$$F_B = F_B^p + F_B^s \tag{5}$$

where the superscript "p" denotes porous NiTi rod. Therefore, the stiffness of the second stage can be derived as

$$S_{A-B} = (F_B - F_A)/(\delta_B - \delta_A) \tag{6}$$

The force–displacement relation for the second stage is given as

$$F_{A-B} = F_A + S_{A-B}(\delta_{A-B} - \delta_A) \tag{7}$$

where $\delta_A \leqslant \delta_{A-B} \leqslant \delta_B$, the subscript "A–B" denotes an arbitrary point between A and B. We will use this manner of notation to express other stages all the way in the following discussion.

3.1.3. The third stage (B → C)

B is the point on which the porous NiTi starts stress-induced martensitic transformation. C is the point at which the porous NiTi rod touches the inner surface of the NiTi spring. Therefore, during this stage the spring and the porous rod are still acting independently. The forces can be obtained in the same manner as for the second stage. The forces and displacements of the porous NiTi rod are given in Table 4. The force in the spring at kink point C is given as

$$F_C^s = E_s[(R_i + t/2)^2 - R_i^2](\delta_C - \delta_B)/(h_p - \delta_B^p) \tag{8}$$

The force applied to the entire composite structure is

$$F_C = F_C^p + F_C^s \tag{9}$$

The stiffness of the third stage is

$$S_{B-C} = (F_C - F_B)/(\delta_C - \delta_B) \tag{10}$$

The force–displacement relation for the third stage is given as

$$F_{B-C} = F_B + S_{B-C}(\delta_{B-C} - \delta_B) \tag{11}$$

where $\delta_B \leqslant \delta_{B-C} \leqslant \delta_C$.

3.1.4. The fourth stage (C → D)

Under increasing compressive loading, the porous NiTi touches the inner surface of the spring which is assumed to be the hollow cylinder at kink point C. From point C thereafter the hollow cylinder and the porous NiTi rod begin to interact to each other, Fig. 6. The composite structure now behaves like a structure of solid cylinder surrounded by a hollow cylinder and their surfaces are touching each other with constraint interface pressure (σ_r^s). The force and displacement relation for solid cylinder will be derived in the following. The equilibrium equation in axi-symmetric cylinder coordinate is given by

$$\frac{d\sigma_{rr}}{dr} + \frac{\sigma_{rr} - \sigma_{\theta\theta}}{r} = 0 \tag{12}$$

Strain–displacement relations are

$$\varepsilon_{rr} = \frac{\partial u}{\partial r}, \quad \varepsilon_{\theta\theta} = \frac{u}{r}, \quad \varepsilon_{zz} = \frac{\partial w}{\partial z} \tag{13}$$

Stress–strain relation in absence of shear component (which is justified due to the assumption of axi-symmetric deformation) is given by

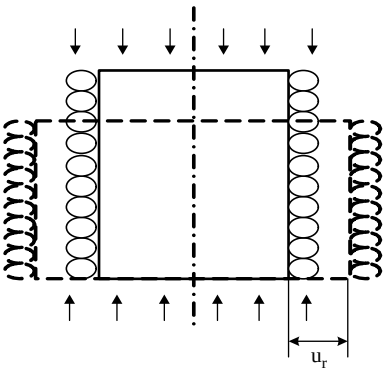

Fig. 6. Porous NiTi rod and NiTi spring interact to each other.

$$\varepsilon_{rr} = \frac{1}{E_i}[\sigma_{rr} - v(\sigma_{\theta\theta} + \sigma_{zz})] \tag{14a}$$

$$\varepsilon_{\theta\theta} = \frac{1}{E_i}[\sigma_{\theta\theta} - v(\sigma_{rr} + \sigma_{zz})] \tag{14b}$$

$$\varepsilon_{zz} = \frac{1}{E_i}[\sigma_{zz} - v(\sigma_{rr} + \sigma_{\theta\theta})] \tag{14c}$$

where subscript "i" denotes NiTi spring (i = s) or porous NiTi cylinder (i = p). From Eq. (14), the stresses can be expressed in terms of strains as

$$\sigma_{rr} = \frac{E_i}{1-v^2}(\varepsilon_{rr} + v\varepsilon_{\theta\theta}) + \frac{v}{1-v}\sigma_0 \tag{15a}$$

$$\sigma_{\theta\theta} = \frac{E_i}{1-v^2}(\varepsilon_{\theta\theta} + v\varepsilon_{rr}) + \frac{v}{1-v}\sigma_0 \tag{15b}$$

$$\sigma_{zz} = \sigma_0 \tag{15c}$$

Replacing the strains with displacements by using Eqs. (13) and (15) given is rewritten as

$$\sigma_{rr} = \frac{E_i}{1-v^2}\left(\frac{\partial u}{\partial r} + v\frac{u}{r}\right) + \frac{v}{1-v}\sigma_0 \tag{16a}$$

$$\sigma_{\theta\theta} = \frac{E_i}{1-v^2}\left(\frac{u}{r} + v\frac{\partial u}{\partial r}\right) + \frac{v}{1-v}\sigma_0 \tag{16b}$$

$$\sigma_{zz} = \sigma_0 \tag{16c}$$

Substituting Eq. (16) into the equilibrium equation (12) we obtain the second-order ordinary differential equation in terms of radial displacement u

$$\frac{d^2u}{dr^2} + \frac{1}{r}\frac{du}{dr} - \frac{u}{r^2} = 0 \tag{17}$$

Eq. (17) is Euler's type differential equation, thus the radial displacement u is given by

$$u_r = Ar \tag{18}$$

where A is an unknown constant.

Substituting Eq. (18) into (16a), we obtain the radial stress in the rod as

$$\sigma_{rr} = \frac{E_i}{1-v^2}A + \frac{v}{1-v}\sigma_0 \tag{19}$$

The radial displacement (u_r^s) of the hollow cylinder subjected to axial stress (σ_0) and lateral pressure (σ_r^s) is given by Arthur et al. (2002)

$$u_r^s = \frac{r}{E_s\left(R_o^2 - R_i^2\right)}\left\{\left[(1-2v) + \frac{(1+v)R_o^2}{r^2}\right]R_i^2\sigma_r^s + v\sigma_0 R_o^2\right\} \tag{20}$$

where u_r^s is the radial displacement of the spring, R_i and R_o are the inner and outer radius of the hollow cylinder, respectively.

There are two unknown in the above formulation, integration constant A in Eqs. (18) and (19) and lateral pressure, σ_r^s. Therefore, we need two boundary conditions to solve these two unknowns. First, the magnitude of the interface pressure, σ_r^s, on the surface of the solid cylinder is equal to that on the inner surface of the hollow cylinder, requiring boundary condition is given as

$$\sigma_r^p|_{r=r_C^p} = \sigma_r^s|_{r=R_i} = \frac{E_p}{1-v^2}A + \frac{v}{1-v}\sigma_0 \tag{21}$$

The second boundary condition is the radial displacement at the surface of the solid cylinder is the same as that at the inner surface of the hollow cylinder, requiring

$$u_r^p\big|_{r=r_c^p} = u_r^s\big|_{r=R_i} \tag{22a}$$

From Eq. (20), the displacement at the inner surface of the hollow cylinder is given by

$$u_r^s\big|_{r=R_i} = \frac{R_i}{E_s(R_o^2 - R_i^2)}\left\{\left[(1-2v)R_i^2 + (1+v)R_o^2\right]\sigma_r^s + v\sigma_0 R_o^2\right\} \tag{22b}$$

The second boundary condition along with Eq. (22b) leads to

$$r_c^p A = \frac{R_i}{E_s\left(R_o^2 - R_i^2\right)}\left\{\left[(1-2v)R_i^2 + (1+v)R_o^2\right]\sigma_r^s + v\sigma_0 R_o^2\right\} \tag{23}$$

Substituting Eq. (21) into Eq. (23) and using relation $r_C^p = R_i$, we can solve for A and σ_r^s

$$A = \frac{v\sigma_0[C_2/(1-v) + R_o^2]}{C_1 - C_2E_p/(1-v^2)} \tag{24a}$$

$$\sigma_r^s = \frac{E_p}{1-v^2}A + \frac{v}{1-v}\sigma_0 \tag{24b}$$

where

$$C_1 = \frac{1}{E_s(R_o^2 - R_i^2)} \tag{25a}$$

$$C_2 = \left[(1-2v)R_i^2 + (1+v)R_o^2\right] \tag{25b}$$

Therefore, the stresses in the rod can be obtained by substituting Eq. (24) into Eq. (16)

$$\sigma_{rr}^i = \frac{E_i}{1-v}A + \frac{v}{1-v}\sigma_0 \tag{26a}$$

$$\sigma_{\theta\theta}^i = -\frac{E_i}{1-v}A + \frac{v}{1-v}\sigma_0 \tag{26b}$$

$$\sigma_{zz} = \sigma_0 \tag{26c}$$

Substituting Eq. (26) into Eq. (14c), the axial strain of the rod can be obtained as

$$\varepsilon_{zz} = \left(1 - \frac{2v^2}{1-v}\right)\frac{\sigma_0}{E_\mathrm{i}} - \frac{2v}{1-v}A \tag{27}$$

The axial strain and stress can be expressed in terms of displacement and force in the z-direction, respectively as

$$\varepsilon_{zz} = \frac{\delta_\mathrm{i}}{h_\mathrm{i}} \tag{28a}$$

$$\sigma_0 = \frac{F_\mathrm{i}}{a_\mathrm{i}} \tag{28b}$$

where δ_i and F_i are the displacement and force in z-direction, respectively, and a_i is the cross area on which the load is applied. The subscript "i" denotes solid cylinder or hollow cylinder. Substituting Eq. (28) into Eq. (27), the force–displacement relation in the solid or hollow cylinder is given as

$$F_\mathrm{i} = \frac{[\delta_\mathrm{i}/h_\mathrm{i} + 2Av/(1-v)]E_\mathrm{i}a_\mathrm{i}}{1 - 2v^2(1-v)} \tag{29}$$

So far, the force–displacement relation for the composite structure when two parts of it interact with each other is obtained. Eq. (29) will be used in all the stages (C–D, D–E, E–F, F–G) when the two parts interact with each other.

For the kink point D, the force in the solid cylinder is given as

$$F_\mathrm{D}^\mathrm{p} = \frac{[(\delta_\mathrm{D} - \delta_\mathrm{C})/h_\mathrm{C}^\mathrm{p} + 2Av/(1-v)]E_\mathrm{D}^\mathrm{p}a_\mathrm{D}^\mathrm{p}}{1 - 2v^2/(1-v)} \tag{30a}$$

The force in the hollow cylinder is

$$F_\mathrm{D}^\mathrm{s} = \frac{[(\delta_\mathrm{D} - \delta_\mathrm{C})/h_\mathrm{C}^\mathrm{s} + 2Av/(1-v)]E_\mathrm{D}^\mathrm{s}a_\mathrm{D}^\mathrm{s}}{1 - 2v^2/(1-v)} \tag{30b}$$

Force in the composite structure is

$$F_\mathrm{D} = F_\mathrm{D}^\mathrm{p} + F_\mathrm{D}^\mathrm{s} \tag{30c}$$

where h_C^i , E_D^i $(\mathrm{i} = \mathrm{p}, \mathrm{s})$ can be found in Table 3. The stiffness of the fourth stage then can be obtained consequently

$$S_\mathrm{C\text{–}D} = (F_\mathrm{D} - F_\mathrm{C})/(\delta_\mathrm{D} - \delta_\mathrm{C}) \tag{31}$$

Therefore the force–displacement relation is given as

$$F_\mathrm{C\text{–}D} = F_\mathrm{c} + S_\mathrm{C\text{–}D}(\delta_\mathrm{C\text{–}D} - \delta_\mathrm{C}) \tag{32}$$

where $\delta_\mathrm{C} \leqslant \delta_\mathrm{C\text{–}D} \leqslant \delta_\mathrm{D}$.

Table 3
Input data for kink points at which the porous NiTi rod and the NiTi spring interact to each other

Kink points		C	D	E	F	G
Height	h^p or h^s (GPa)	14.50 mm	14.08 mm	13.25 mm	14.10 mm	14.5 mm
Young's Modulus	E^p	9	23	23	9	9
	E^s	70	70	70	70	70

Table 4
Displacement and forces of kink points in the FDC (F_i^P and δ_i^P) of porous NiTi rod and spring where "i" denotes kink point from A to I; δ^i is the displacement of composite structure

Kink points in Fig. 5		A	B	C	D	E	F	G	H	I
Displacement	δ_i^P (mm)	0.00	0.45	0.50	0.92	1.75	0.90	0.50	0.02	0.00
	δ_i (mm)	5.30	5.75	5.80	6.22	7.05	6.20	5.80	5.32	5.30
Force	F_i^P (KN)	N/A	14.00	15.00	N/A	N/A	N/A	N/A	5.00	N/A

F_i^P is the force of single porous NiTi rod.

3.1.5. The fifth stage ($D \rightarrow E$)

Kink point D is the martensitic finish transformation point for the porous NiTi rod. From D all the way to E, the porous NiTi rod is in 100% martensite phase. As a result, the Young's modulus of the porous NiTi rod at this stage is the martensite Young's modulus of 13% porosity NiTi [12]. While for the NiTi spring, its Young's modulus is to be 70 GPa. Because the solid cylinder (porous NiTi rod) and the hollow cylinder (NiTi spring) is still interacting with each other in this stage. The forces in the cylinders can be obtained in the same way as that for the fourth stage. The forces at E are given as

$$F_E^p = \frac{[(\delta_E - \delta_D)/h_D^p + 2Av/(1-v)]E_E^p a_E^p}{1 - 2v^2/(1-v)} \quad \text{(solid cylinder)} \tag{33a}$$

$$F_E^s = \frac{[(\delta_E - \delta_D)/h_D^s + 2Av/(1-v)]E_E^s a_E^s}{1 - 2v^2/(1-v)} \quad \text{(hollow cylinder)} \tag{33b}$$

$$F_E = F_E^p + F_E^s \quad \text{(composite structure)} \tag{33c}$$

where h_D^i , E_E^i (i = p, s) can be found in Table 3. The stiffness of the fifth stage is

$$S_{D\text{-}E} = (F_E - F_D)/(\delta_E - \delta_D) \tag{34}$$

The force–displacement relation is given as

$$F_{D\text{-}E} = F_D + S_{D\text{-}E}(\delta_{D\text{-}E} - \delta_D) \tag{35}$$

where $\delta_D \leqslant \delta_{D\text{-}E} \leqslant \delta_E$.

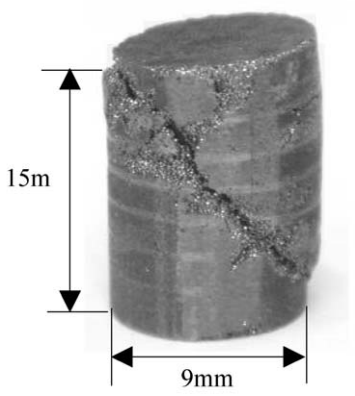

Fig. 7. Fractured 13% porous NiTi rod.

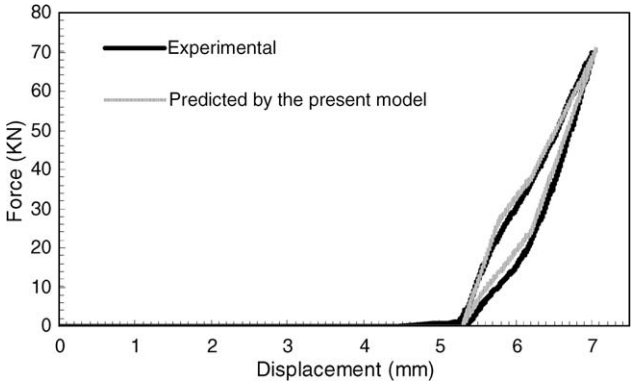

Fig. 8. Experimental and predicted force–displacement curve.

3.2. Unloading curve

The unloading curve consists five stages (E–F, F–G, G–H, H–I, I–O) and five kink points (E, F, G, H, I). In the first two stages (E–F, F–G), the porous NiTi rod and NiTi spring are still constraining each other. The force–displacement curve for these two stages are obtained in the same way as that for the fourth (C–D) and fifth (D–E) stage in the loading curve. In the other three stages (G–H, H–I, I–O), the porous NiTi rod and NiTi spring deform independently with same gap between them. Therefore, their FDCs are obtained in the same way as that for the first (O–A), second (A–B) and third (B–C) stage in the loading curve. The detailed computation is in Appendix A.

4. Discussion

The actual stress distribution in the cross-section of the spring is shown in Fig. 9, but to simplify the problem, we assume that when the neighbor turn of the spring touches each other it acts like a hollow cylinder (Fig. 6). We assume that the Young's modulus of the spring is 70 GPa all the way, but the

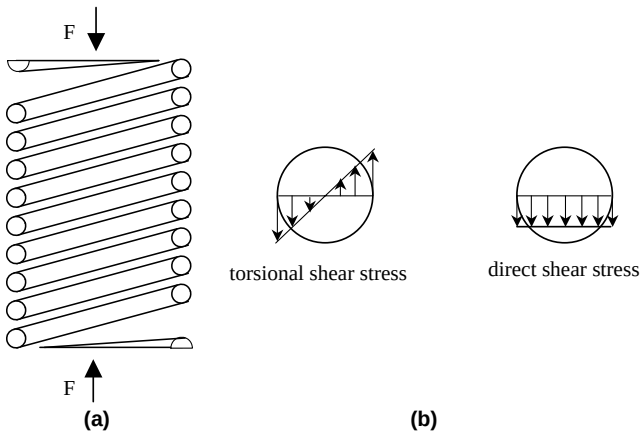

Fig. 9. (a) Axially loaded helical spring and (b) free-body diagram showing that the wire is subjected to a direct shear and a torsional shear.

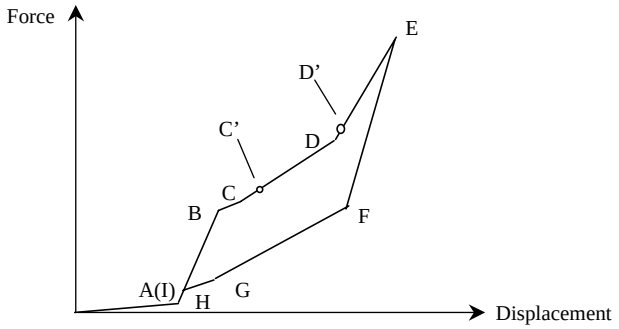

Fig. 10. Idealized force–displacement curve of the composite structure.

Von-Mises effect stress of the spring shows the fact that when the force arrives point C′ on the curve in Fig. 10, stress-induced transformation starts in the NiTi spring, and the martensitic transformation finishes at point D′. Therefore, this model is more accurate before the force hits C′ and after the force increases over D′. For the stress-induced martensite transformation stage of the NiTi spring, this model is over estimate.

This hollow cylinder assumption allows the discrete spring turns to be a continuous body, therefore strengthens the effect of the spring. Comparing the predicted curve to the experimental curve in Fig. 8, we can see that with the force and displacement increasing, the gap between those two curves narrows. That is because with the force increasing, the turns of the spring are compressed more and more tightly to each other, that makes the spring more and more like a hollow cylinder with continuous wall. Therefore, the proposed model even if it is based on simple elastic theory, can predict the force–displacement of the experimental data accurately.

Fig. 7 shows that the fracture occurs in the plane 45° to the axial load, which coincides with the maximum shear stress plane (Brooks and Choudhury (2002)). The force–displacement of the single porous NiTi rod does not exhibit a sufficiently long plastic plateau before it fractures. There are three reasons. First, this is partially due to the characteristics associated with the NiTi of SE grade supplied by Sumitomo Metals where the NiTi powders of SE grade may not exhibit extensive plastic deformation with marked plastic stress plateau. Second, it is probably because that the pores in the porous NiTi rod weaken the ductility of the rod. Third, part of interconnects of the NiTi particles by the SPS were weakened or destroyed by the heave compressive load.

Comparison of the specific EA of some ordinary materials to that of the single NiTi rod and composite structure, Table 5, shows that the single NiTi rod has more than 10 times specific EA as ordinary materials based on the EA/(unit volume). Moreover, the EA of the proposed composite structure made of a porous NiTi rod surrounded by a concentric NiTi spring is more than twice as much as that of the single NiTi rod. Therefore, the proposed composite structure in this paper has a remarkable advantage

Table 5
Comparison of the specific EA of various materials

Materials	$AlCu_4$ foam (Baumeister et al., 1997)	Al with Si added (Du et al., 2003)	Al (Ashby et al., 2000)	Single 13% porosity NiTi rod	Composite structure
Energy absorption (MJ/m^3)	5.2	4.2	20	68.3	141.5

for use as a high energy absorber. However, on the basis of EA/(unit weight) the large advantage of the proposed composite structure diminishes as compared with Al foam, i.e. the composite has 15.3 MJ/Mg, Al foam has 10 MJ/Mg (Ashby et al., 2000). The reason for this small advantage of the proposed NiTi composite structure over Al foam in terms of EA/(unit weight) is that the porosity of the proposed NiTi composite structure, particularly porous NiTi rod, is not as high as 50% or more. For such a high porosity NiTi rod, the thin NiTi wall of the porous microstructure may not undergo large stress and strain region, instead, if may exhibit a buckling mode limiting the volume of large stress and strain in a localized hinged area.

5. Conclusion

The proposed composite structure composed of porous NiTi rod surrounded by a concentric NiTi spring, exhibits high force and displacement relation as compared with that of the single porous NiTi rod with the identical dimension. Therefore, this composite structure has higher specific energy absorption than that of the single porous NiTi rod. The force–displacement curve of the composite structure predicted by the proposed model explains the experimental data reasonably, Fig. 8.

Acknowledgements

The present research was supported by a subcontract from the ONR-MURI at University of California at San Diego (PI, Prof. Sia Nemat-Nasser, N-000140210666) to the University of Washington where Dr. Roshdy Barsoum is the program monitor at ONR. The authors are thankful to Dr. Y. Urushiyama for his valuable comments on the design of the composite structure.

Appendix A. Unloading curve

A.1. The sixth stage ($E \to F$)

The force and displacement at point E is obtained in Eq. (33c). Point F is the austenite transformation start point. The force at point F is

$$F_{\mathrm{F}}^{\mathrm{p}} = \frac{[(\delta_{\mathrm{F}} - \delta_{\mathrm{E}})/h_{\mathrm{E}}^{\mathrm{p}} + 2Av/(1-v)]E_{\mathrm{F}}^{\mathrm{p}} a_{\mathrm{F}}^{\mathrm{p}}}{1 - 2v^2/(1-v)} \quad \text{(solid cylinder)} \tag{A.1}$$

$$F_{\mathrm{F}}^{\mathrm{s}} = \frac{[(\delta_{\mathrm{F}} - \delta_{\mathrm{E}})/h_{\mathrm{E}}^{\mathrm{s}} + 2Av/(1-v)]E_{\mathrm{F}}^{\mathrm{s}} a_{\mathrm{F}}^{\mathrm{s}}}{1 - 2v^2/(1-v)} \quad \text{(hollow cylinder)} \tag{A.2}$$

$$F_{\mathrm{F}} = F_{\mathrm{F}}^{\mathrm{p}} + F_{\mathrm{F}}^{\mathrm{s}} \quad \text{(composite structure)} \tag{A.3}$$

The stiffness of the sixth stage is

$$S_{\mathrm{E-F}} = (F_{\mathrm{F}} - F_{\mathrm{E}})/(\delta_{\mathrm{F}} - \delta_{\mathrm{E}}) \tag{A.4}$$

The force–displacement relation is given as

$$F_{\mathrm{E-F}} = F_{\mathrm{E}} + S_{\mathrm{E-F}}(\delta_{\mathrm{E-F}} - \delta_{\mathrm{E}}) \tag{A.5}$$

where $\delta_{\mathrm{F}} \leqslant \delta_{\mathrm{E-F}} \leqslant \delta_{\mathrm{E}}$.

A.2. The seventh stage ($F \rightarrow G$)

Point G is the point at which the porous NiTi rod detaches the spring, while the porous NiTi rod is still at the stress-induced martensite stage. Therefore, its stiffness is still 9 GPa in this stage, Table 3. The force at point F is

$$F_{\mathrm{G}}^{\mathrm{p}} = \frac{((\delta_{\mathrm{G}} - \delta_{\mathrm{F}})/h_{\mathrm{F}}^{\mathrm{p}} + 2Av/(1-v))E_{\mathrm{G}}^{\mathrm{p}}a_{\mathrm{G}}^{\mathrm{p}}}{1 - 2v^2/(1-v)} \tag{A.6}$$

$$F_{\mathrm{G}}^{\mathrm{p}} = \frac{((\delta_{\mathrm{G}} - \delta_{\mathrm{F}})/h_{\mathrm{F}}^{\mathrm{s}} + 2Av/(1-v))E_{\mathrm{G}}^{\mathrm{s}}a_{\mathrm{G}}^{\mathrm{s}}}{1 - 2v^2/(1-v)} \tag{A.7}$$

$$F_{\mathrm{F}} = F_{\mathrm{F}}^{\mathrm{p}} + F_{\mathrm{F}}^{\mathrm{s}} \tag{A.8}$$

The stiffness of the seventh stage is given as

$$S_{\mathrm{F-G}} = (F_{\mathrm{G}} - F_{\mathrm{F}})/(\delta_{\mathrm{G}} - \delta_{\mathrm{F}}) \tag{A.9}$$

The force–displacement relation is given as

$$F_{\mathrm{F-G}} = F_{\mathrm{F}} + S_{\mathrm{F-G}}(\delta_{\mathrm{F-G}} - \delta_{\mathrm{F}}) \tag{A.10}$$

where $\delta_{\mathrm{G}} \leqslant \delta_{\mathrm{F-G}} \leqslant \delta_{\mathrm{F}}$.

A.3. The eighth stage ($G \rightarrow H$)

From point G, the rod detaches from the inner surface of the spring. Therefore, the hollow cylinder and the solid cylinder act independently from point G all the way to original point O. Point H is the point at which the austenite transformation finishes. The force at point H is

$$F_{\mathrm{H}}^{\mathrm{s}} = E_{\mathrm{s}}\lfloor(R_{\mathrm{i}} + t/2)^2 - R_{\mathrm{i}}^2\rfloor(\delta_{\mathrm{G}} - \delta_{\mathrm{H}})/(h_{\mathrm{p}} - \delta_{\mathrm{G}}^{\mathrm{p}}) \tag{A.11}$$

$$F_{\mathrm{H}} = F_{\mathrm{H}}^{\mathrm{p}} + F_{\mathrm{H}}^{\mathrm{s}} \tag{A.12}$$

where the $F_{\mathrm{H}}^{\mathrm{p}}$ is given in Table 4.

The stiffness of the eighth stage is given as

$$S_{\mathrm{G-H}} = (F_{\mathrm{H}} - F_{\mathrm{G}})/(\delta_{\mathrm{H}} - \delta_{\mathrm{G}}) \tag{A.13}$$

The force–displacement relation is given as

$$F_{\mathrm{G-H}} = F_{\mathrm{G}} + S_{\mathrm{G-H}}(\delta_{\mathrm{G-H}} - \delta_{\mathrm{F}}) \tag{A.14}$$

where $\delta_{\mathrm{H}} \leqslant \delta_{\mathrm{G-H}} \leqslant \delta_{\mathrm{G}}$.

A.4. The ninth stage ($H \rightarrow I$)

The porous NiTi rod recovers completely to its original height at point I. That means that from point I, only the spring is taking the load. Therefore, the point I has the same value as point A, and the force of the composite structure at point A is the same as the force only in spring at point A

$$F_{\mathrm{I}} = F_{\mathrm{A}}^{\mathrm{s}} = \frac{G_{\mathrm{s}}d^2}{64nR_{\mathrm{o}}^2}\delta_{\mathrm{A}} \tag{A.15}$$

The stiffness of the eighth stage is given as

$$S_{\mathrm{H-I}} = (F_{\mathrm{I}} - F_{\mathrm{H}})/(\delta_{\mathrm{I}} - \delta_{\mathrm{H}}) \tag{A.16}$$

The force–displacement relation is

$$F_{H-I} = F_H + S_{H-I}(\delta_{H-I} - \delta_H) \tag{A.17}$$

where $\delta_I \leqslant \delta_{H-I} \leqslant \delta_H$.

A.5. The ninth stage ($I \rightarrow O$)

Since point I is the same point as point A. The force–displacement curve overlaps to the first stage ($O \rightarrow A$).

References

Ashby, M.F., Evans, A.G., Fleck, N.A., Gibson, L.J., Hutchinson, J.W., Wadley, H.N.G., 2000. Metal Foams: A Design Guide. Butterworth Heinemann, Boston.

Bart-Smith, H., Hutchinson, J.W., Evans, A.G., 2001. Measurement and analysis of the structural performance of cellular metal sandwich construction. International Journal of Mechanical Sciences 43, 1945–1963.

Baumeister, J., Banhart, J., Weber, M., 1997. Aluminum foams for transport industry. Materials and Designs 18 (4), 217–220.

Brooks, C.R., Choudhury, A., 2002. Failure Analysis of Engineering Materials. McGraw-Hill Publication.

Du, H., Lee, S.W., Sun, C., Wen, L.S., 2003. Effect on compression properties of Al alloy foam materials by added Si. Materials Science Forum 439, 282–288.

Kang, Y.S., Kikuchi, K., Kawasaki, A., 2001. Fabrication and characterization of functionally graded Ni/Al2O3/Ni compliant pad. In: Proceeding of ISSPS, Japan.

Kassapoglou, C., 1996. Compression strength of composite sandwich structures after barely visible impact damage. Journal of Composites Technology and Research 18 (4), 272–284.

Kato, H., Koyari, T., Tokizane, M., Miura, S., 1994. Stress–strain behavior and shape memory effect in powder metallurgy TiNi alloys. Acta Metallurgica et Materialia 42 (4), 1351–1358.

Kusaka, M., Taya, M., 2004. Design of ferromagnetic shape memory alloy composites. Journal of Composite Materials 38 (12), 1011–1035.

Miyoshi, T., Itoh, M., Mukai, T., Kanahashi, H., Kohzu, H., Tanabe, S., Higashi, K., 1999. Enhancement of energy absorption in closed-cell aluminum by the modification of cellular structures. Scripta Materialia 41 (10), 1055–1060.

Wicks, N., Hutchinson, J.W., 2001. Optimal truss plates. International Journal of Solids and Structures 38, 5165–5183.

Wicks, N., Hutchinson, J.W., 2004. Performance of sandwich plates with truss cores. Mechanics of Materials 36, 739–751.

Xue, Z.Y., Hutchinson, J.W., 2004. A comparative study of impulse-resistant metal sandwich plates. International Journal of Impact Engineering 30, 1283–1305.

Zhao, Y., Taya, M., Kang, Y.S., Kawasaki, A., 2005. Compressive behavior of porous NiTi shape memory alloys. Acta Materialia 53, 337–343.